

# Computing the Distance between unbalanced Distributions- The flat Metric

Henri Schmidt<sup>1\*†</sup> and Christian Düll<sup>1†</sup>

<sup>1</sup>Institute of Mathematics, Heidelberg University, Im Neuenheimer Feld  
205, 69120, Heidelberg, Germany.

\*Corresponding author(s). E-mail(s): [henri.schmidt@posteo.de](mailto:henri.schmidt@posteo.de);

Contributing authors: [duell@math.uni-heidelberg.de](mailto:duell@math.uni-heidelberg.de);

<sup>†</sup>These authors contributed equally to this work.

## Abstract

We provide an implementation to compute the flat metric in any dimension. The flat metric, also called dual bounded Lipschitz distance, generalizes the well-known Wasserstein distance  $W_1$  to the case that the distributions are of unequal total mass. This is of particular interest for unbalanced optimal transport tasks and for the analysis of data distributions where the sample size is important or normalization is not possible. The core of the method is based on a neural network to determine an optimal test function realizing the distance between two given measures. Special focus was put on achieving comparability of pairwise computed distances from independently trained networks. We tested the quality of the output in several experiments where ground truth was available as well as with simulated data.

**Keywords:** flat norm, dual bounded Lipschitz distance, Fortet-Mourier distance, unbalanced optimal transport

## 1 Introduction

This paper is devoted to the implementation of a method for computing the flat metric between two nonnegative Radon measures of potentially unequal total mass, realized by a neural network. Special focus lies on an implementation which works in any dimension as well as comparability of pairwise computed distances from independently trained networks.

In this paper, we will consider measures with different masses, so that we work in  $\mathcal{M}^+(\mathbb{R}^d)$ , i.e. the cone of nonnegative, bounded real-valued Borel measures on  $\mathbb{R}^d$ . We equip  $\mathcal{M}^+(\mathbb{R}^d)$  with the **flat metric** (or **dual bounded Lipschitz distance**, **Fortet-Mourier distance**) defined by

$$\rho_F(\mu, \nu) = \sup_{\|f\|_{BL} \leq 1} \int_{\mathbb{R}^d} f \, d(\mu - \nu) = \sup_{\|f\|_{BL} \leq 1} \mathbb{E}_{x \sim \mu}[f(x)] - \mathbb{E}_{x \sim \nu}[f(x)]. \quad (1.1)$$

The class of test functions is given by the bounded Lipschitz functions endowed with the norm

$$\|f\|_{BL} = \max(\|f\|_{\infty}, |f|_{\text{Lip}}),$$

where  $\|f\|_{\infty} = \sup_{x \in \mathbb{R}^d} |f(x)|$  and  $|f|_{\text{Lip}} = \sup_{x \neq y} \frac{|f(x) - f(y)|}{|x - y|}$ . Note that formulation (1.1) resembles the Kantorovich-Rubinstein duality of the Wasserstein distance  $W_1$ , i.e.

$$W_1(\mu, \nu) = \sup_{|f|_{\text{Lip}} \leq 1} \int_{\mathbb{R}^d} f \, d(\mu - \nu). \quad (1.2)$$

Coming from optimal transport theory [Cuturi \(2013\)](#); [Villani \(2003, 2009\)](#), the Wasserstein metrics define distances between probability measures which take into account the geometry of the underlying state space. Consequently, distances with respect to the Wasserstein metrics are more robust [Grauman and Darrell \(2004\)](#); [Ling and Okada \(2007\)](#); [Peyré et al \(2012\)](#); [Villani \(2003, 2009\)](#). Note that the Wasserstein distances scale with the total mass of the measures  $\mu, \nu$  and are thus not necessarily restricted to probability measures. However, by construction the distances are only applicable in conservative problems, i.e. only if  $\mu(\mathbb{R}^d) = \nu(\mathbb{R}^d)$ , as otherwise no optimal transport plan exists, see e.g. ([Ulikowska, 2013](#), Remark 1.18).

In cases where the measures or data distributions can not be normalized as the mass differences are meaningful, which is the case in color transfer, for example, other approaches are necessary to handle these so-called unbalanced optimal transport tasks. In [Schiebinger et al \(2019\)](#); [Zhang et al \(2021\)](#) the authors employed the (entropically regularized) Wasserstein metric to compute distances between single cell mRNA distributions of cell samples and to infer developmental trajectories. However, as the inherent cell growth leads to an unbalanced transport problem, the data had to be renormalized with an additional model function accounting for cell growth. Such a renormalization could have been avoided if the authors had used a metric which is able to handle measures with different mass, see [Chizat et al \(2018\)](#); [Peyré and Cuturi \(2019\)](#) for an overview of several approaches on unbalanced optimal transport. From the purely theoretical side, the obvious candidate would be given by the well-established total variation norm

$$\|\mu\|_{TV} := \mu^+(\mathbb{R}^d) + \mu^-(\mathbb{R}^d),$$

where  $\mu^+, \mu^-$  are the measures arising from Jordan decomposition theorem (Folland, 1984, Theorem 3.4). However, as the corresponding topology is too strong and completely ignores the underlying geometry, the  $\|\cdot\|_{TV}$  norm is basically useless. For instance the distance between two Dirac measures is given by

$$\|\delta_a - \delta_b\|_{TV} = \delta_a(\mathbb{R}^d) + \delta_b(\mathbb{R}^d) = 2 \quad \forall a, b \in \mathbb{R}^d, a \neq b.$$

So instead we choose the flat metric which generates a weaker topology and has convenient analytical properties, providing completeness and separability for the measure space  $\mathcal{M}^+(\mathbb{R}^d)$  Düll et al (2022); Gwiazda et al (2018). In contrast to the widespread Kullback-Leibler divergence and its relatives  $\rho_F$  actually defines a distance which simplifies interpretability of the distances. Furthermore, the following alternative characterization of the flat metric due to Piccoli and Rossi (Piccoli and Rossi, 2014, Theorem 13)

$$\rho_F(\mu, \nu) = \inf_{\substack{\tilde{\mu} \leq \mu, \tilde{\nu} \leq \nu \\ \|\tilde{\mu}\|_{TV} = \|\tilde{\nu}\|_{TV}}} \|\mu - \tilde{\mu}\|_{TV} + \|\nu - \tilde{\nu}\|_{TV} + W_1(\tilde{\mu}, \tilde{\nu}). \quad (1.3)$$

shows that the flat metric is a suitable generalization of the 1-Wasserstein distance  $W_1$  for unbalanced tasks and as such distances with respect to  $\rho_F$  are also geometrically faithful, at least locally (see 3.2). The decomposition (1.3) into terms with total variation and the term with Wasserstein distance admits a heuristic interpretation: Any share  $\delta\mu$  of the mass of  $\mu$  can either be transported from  $\mu$  to  $\nu$  at cost  $W_1(\delta\mu, \delta\nu)$  or removed at cost  $\|\delta\mu\|_{TV}$ . As such, the minimal "sub-measures"  $\tilde{\mu}, \tilde{\nu}$  achieve an optimal compromise between mass transportation and cancellation.

The flat metric has been used in Lellmann et al (2014) for inverse problems in imaging and recently to establish well-posedness theory for structured population models in measures on separable and complete metric spaces Düll et al (2022).

## 2 Methods

Given two measures  $\mu, \nu \in \mathcal{M}^+(\mathbb{R}^d)$ , explicitly computing their flat distance via (1.1) is highly nontrivial as finding a closed analytical expressions for the flat metric proves to be complicated even for Dirac measures, see Proposition 1. So instead we trained a neural network of two fully connected hidden layers with 64 neurons each and the Adam optimizer Kingma and Ba (2015) to approximate  $\rho_F(\mu, \nu)$  using (1.1). Note that we deliberately chose a shallow network architecture as it provides sufficiently good results whereas moving to larger networks results in instabilities or even failures during training due to limited training data. In view of the Universal Approximation Theorem proven in Anil et al (2019), a suitable choice of architectural constraints allows the whole space  $BL(\mathbb{R}^d)$  to be accessed via the network, so that we can expect meaningful results.

We make the ansatz  $f = f_\Theta$  and model the optimal bounded Lipschitz test function by a multi-layer perceptron. To ensure that  $f_\Theta$  is indeed admissible to the problem, i.e. that it is a bounded Lipschitz function with  $\|\cdot\|_{BL}$  norm bounded by 1, we use a mixed approach of regularization and architectural constraints. In particular, we

adopt the architectural approach introduced in [Anil et al \(2019\)](#) to guarantee Lipschitz continuity whereas we use regularizational constraints to account for the optimization problem (1.1) and to enforce boundedness of  $f_\Theta$ .

**Architectural constraints:** In [Anil et al \(2019\)](#) the authors Anil, Lucas and Grosse constructed a neural network to calculate the Wasserstein distance  $W_1$  via its Kantorovich-Rubinstein duality (1.2). Their approach is based on the fact that Lipschitz continuity is closed under compositions, so that it is sufficient to control the Lipschitz constant of each individual layer and activation function. In order to compute  $W_1$  Anil, Lucas and Grosse proposed to normalize each layer  $A_i$  and to use the 1-Lipschitz shuffling operator **GroupSort** [Chernodub and Nowicki \(2017\)](#) as activation function. This way the authors are able to construct a universal Lipschitz approximator. Hence, adopting the network architecture will yield Lipschitz continuity of  $f_\Theta$ . We shortly summarize the most important concepts of the paper.

In [Anil et al \(2019\)](#) the authors apply Björck orthonormalization [Björck and Bowie \(1971\)](#) during each forward pass which ensures that the linear transformation induced by layer  $A_i$  is in fact isometric, thus strictly enforcing  $|A_i|_{\text{Lip}} = 1$ . While this is convenient for the computation of  $W_1$  as the test function  $f$  will always be 1-Lipschitz theoretically, in our setting a Björck orthonormalization is too restrictive as in practice the optimal  $f_\Theta$  of the flat distance often has a smaller Lipschitz constant  $|f_\Theta|_{\text{Lip}}$ . Thus, in our implementation we necessarily have to switch to **spectral normalization**  $\|A_i\|_2 = 1$  instead which ensures that the largest singular value is 1 but there may be other eigenspaces with smaller absolute singular values. In particular, we do not require  $A_i$  to be 1-Lipschitz in every direction but just enforce  $|A_i|_{\text{Lip}} \leq 1$ . As the spectral normalization- in contrast to Björck orthonormalization- is not gradient norm preserving, our choice potentially leads to diminishing gradient norms of the network during backpropagation and thus to slower convergence of the network, see ([Anil et al, 2019](#), B.2).

Nevertheless, the Björck and the spectral normalization yield similar results for a simple toy problem presented in Figure 1. In particular, the Björck approach is also able to produce gradients with norm less than one between probability measures  $\mu, \nu$ . This is rather surprising as in the Wasserstein case (i.e. without a bound constraint in the loss)  $f_\Theta$  should indeed attain  $|\nabla f_\Theta| = 1$  due to the linear 1-Lipschitz layers, see also ([Gulrajani et al, 2017](#), Corollary 1). We assume that the bound constraint (2.3) interferes with the normalization, such that the linear layers are in fact not completely orthonormal.

The activation function **GroupSort** is a nonlinear, 1-Lipschitz operator which generalizes *ReLU* [Anil et al \(2019\)](#). It separates the pre-activations into groups and within each group permutes the input yielding an isometry. Typically, we will use two pre-activations per group, though higher values can be chosen too. In contrast to ReLU, GroupSort prevents gradient norm attenuation which would lead to  $|f_\Theta|_{\text{Lip}} \ll 1$  for deep networks. It often arises as a ReLU unit will map half of its input space to zero, thereby effacing all of the previous layers' gradients in this region. In fact, it can be shown that a weight-constraint and norm-preserving neural network with ReLU activations is in fact linear, [Anil et al \(2019\)](#). Due to the lack of computational complexity, such a network is undesirable and thus the challenge is to construct a neural network

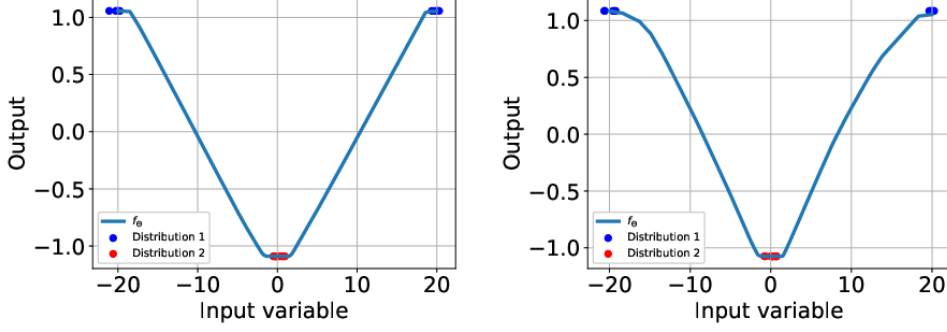


**Fig. 1** A simple 1D experiment showing the similarities between spectral normalization (left) and Björck orthonormalization (right). We considered two Gaussian mixture models  $\mu = \frac{128}{2}(\mathcal{N}(-20, 0.5) + \mathcal{N}(20, 0.5))$  (blue) and  $\nu = 128\mathcal{N}(0, 0.5)$  (red). In both cases the resulting  $f_\Theta$  was plotted. Each time  $f_\Theta$  is bounded and  $|f_\Theta|_{\text{Lip}} \ll 1$

which is 1-Lipschitz and simultaneously maintains enough expressive power to be a universal approximator. Both, in the work by Anil et al. [Anil et al \(2019\)](#) and our work GroupSort has proven to work well while preserving enough expressive power to be a universal approximator.

Note that in view of [Tsuzuku et al \(2018\)](#) a Lipschitz constrained network provides provable adversarial robustness, i.e. the change in output under small adversarial perturbations is bounded.

**Regularization constraints:** Our loss term has to account for both the optimization problem of the flat metric and the boundedness constraint for  $f_\Theta$ , so that the **total loss term**  $\mathcal{L}$  consists of two parts

$$\mathcal{L} := \mathcal{L}_m + \lambda \mathcal{L}_b. \quad (2.1)$$

The **metric loss** term  $\mathcal{L}_m$  corresponds to minimizing the negative of (1.1) and is given by

$$\mathcal{L}_m := -\mathbb{E}_{x \sim \mu}[f_\Theta(x)] + \mathbb{E}_{x \sim \nu}[f_\Theta(x)]. \quad (2.2)$$

Note that after training  $\mathcal{L}_m$  approximately yields the negative value of the flat distance  $\rho_F(\mu, \nu)$ .

The additional penalty term to bound  $f_\Theta$  is provided by the **bound loss term**

$$\mathcal{L}_b \left( \frac{1}{\|\mu\|_{TV}} \langle h_\mu, h_\mu \rangle + \frac{1}{\|\nu\|_{TV}} \langle h_\nu, h_\nu \rangle \right), \quad (2.3)$$

where  $h_\kappa := \max_{x \sim \kappa} (|f_\Theta(x)| - M, 0)$  and the parameter  $M$  refers to the upper bound for  $\|f_\Theta\|_\infty$  which in our formulation is given by  $M = 1$ . By choosing this approach over simply considering the maximal value  $\|f_\Theta\|_\infty$ , we reduce the effect of outliers in the data simplifying training. The auxiliary functions  $h_\kappa$  encode in which areas

$f_\Theta$  deviates from its target bound evaluated each on the input given by  $\kappa = \mu$  and  $\kappa = \nu$  respectively. If such a deflection  $|f_\Theta| > 1 = M$  occurs, the corresponding  $h_\kappa$  will have non-vanishing values in the appropriate domain and  $h_\kappa$  serves as a penalty. The penalties are then accumulated over the whole space by the inner product  $\langle \cdot, \cdot \rangle$  which thus measures how much  $f_\Theta$  violates the bound when evaluated with respect to  $\mu$  and  $\nu$  respectively. As the loss term should not favour measures with large total masses, we normalize each contribution by its respective total variation ensuring that the penalty terms remain invariant under scaling of the total mass. This will be useful as our implementation only considers discrete measures where the total variation is simply the number of support points so that it doesn't matter whether the same empiric distribution is given 100 or 1000 data points.

The two penalty contributions with respect to  $\mu$  and  $\nu$  are then combined to give the overall penalty  $\mathcal{L}_b$  incurred by violating bound  $M$ . In practice, enforcing the ideal bound of a vanishing  $\mathcal{L}_b$  is not possible in general and hence we strive for small values of the loss. Due to the inner product, penalty contributions enter quadratically in  $\mathcal{L}_b$  punishing larger deviations from  $M$  more severely than smaller ones.

As 1— Lipschitz continuity of  $f_\Theta$  will be guaranteed by the network architecture, the combined loss  $\mathcal{L}$  then accounts for both rendering  $f_\Theta$  admissible to the optimization problem (1.1) as well as finding the optimal value of the flat metric. Such an approach of having one loss term for the problem and one for the admissibility is commonly employed, e.g in the implementation of Wasserstein gradient-penalty adversarial networks Gulrajani et al (2017). We remark that in (2.1) both contributions act antagonistically as a decrease in  $\mathcal{L}_m$  often leads to an increase in  $\mathcal{L}_b$ , see Figure 9 where the individual loss terms are monitored during training.

Note that the two loss contributions  $\mathcal{L}_m$  and  $\mathcal{L}_b$  of  $\mathcal{L}$  in (2.1) are effectively balanced by an enforcing parameter  $\lambda = \lambda(t)$  which depends on the fraction of elapsed training  $t$ . Specifically,  $\lambda$  is chosen *adaptively* so that each freshly trained network is approximately bound by the same constant  $\|f_\Theta\|_\infty \leq M$  while simultaneously having comparable relative loss contributions of  $\mathcal{L}_m$  and  $\mathcal{L}_b$  regardless of the input distributions. This is particularly important for our setting as we want to establish pairwise comparisons of neural networks which have been trained independently and/or on different data sets. This regularly occurs when computing pairwise distances between subdistributions so that the output of the network should be ordinal. Without proper balancing the resulting  $f_\Theta$  will adhere more or less strict to the  $\|\cdot\|_\infty$  bound depending on the currently dominating loss term leading to biased results. Notably, different networks would solve different optimization problems (1.1) yielding their actual outcomes to be incomparable to each other. To be more specific, we can not simply set  $\lambda$  sufficiently large such that the bound constraint  $\|f_\Theta\|_\infty \leq 1 = M$  is guaranteed to be satisfied. Instead, we incorporated checks at various points during training, at which we update the enforcing parameter  $\lambda$  dynamically. Details to this procedure are listed in Appendix A.

**Implementation** This paper and the corresponding code is based on the work by Anil, Lucas, and Grosse in Anil et al (2019). We forked their Github repository and adjusted it to our purposes. All our code can be found at <https://github.com/hs42/flat-metric> together with helpful beginner guides, examples and visualization tools.

The code itself uses the PyTorch framework with unsupervised training. Notice that only the bound loss  $\mathcal{L}_b$  acts as an error measure and should thus vanish after training whereas the metric loss  $\mathcal{L}_m$  essentially becomes the estimator for the flat distance  $\rho_F \approx -\mathcal{L}_m$  and hence ought to persist.

The chosen network architecture of two fully connected hidden layers with 64 neurons each and the Adam optimizer [Kingma and Ba \(2015\)](#) turned out to provide good results while moving to larger networks results in instabilities due to scarcity of training data for small distributions. In particular, the computed validation loss agrees well with the training loss and thus we conclude that our simple setup is powerful enough to generalize on the provided training set. This way, we can account for the inherent noise of experimental data and prevent overfitting. Further experiments concerning the performance of the network architecture can be found in [Section B.5](#).

### 3 Experiments

With our experiments we want to quantify whether our proposed methods are suitable for determining the flat distance between measures and to investigate the performance of our implementation. To this end, we first consider situations in which we are able to provide analytical ground truth. Unfortunately, such results are difficult to find and hence we are restricted to comparatively simple distributions for our analysis, see [Proposition 1](#). In a second step, we look at high dimensional simulated data.

When computing the flat distance between two measures  $\mu, \nu$ , we scale the loss  $\mathcal{L}_m$  by the smaller of the two total masses for simplicity. In particular, we assume that at least one is a probability measure and the other one has total mass of at least one. The loss  $\mathcal{L}_m$  is thus computed as

$$\mathcal{L}_m = -\frac{1}{K} \left[ \sum_{i=1}^{N_\mu} f_\Theta(s_i^\mu) - \sum_{i=1}^{N_\nu} f_\Theta(s_i^\nu) \right], \quad (3.1)$$

where  $\{s_1^\mu, \dots, s_{N_\mu}^\mu\}$  and  $\{s_1^\nu, \dots, s_{N_\nu}^\nu\}$  denote the data samples of  $\mu$  and  $\nu$  respectively and  $K = \min\{N_\mu, N_\nu\}$ . For further technical details we refer to our Github repository.

#### 3.1 Toy experiment: The distance of the supports

In this series of experiments, one measure will always be a Dirac measure with mass  $n$  concentrated at the origin  $\mu = n\delta_0$  whereas the other one is given by a linear combination of  $m$  Diracs  $\nu = \sum_{i=1}^m \delta_{x_i}$  concentrated at points  $x_i \in \mathbb{R}^d$ . Further experimental details are provided in [Appendix B](#). As a start we take two measures with the same total mass, i.e.  $n = m$  and randomly sample  $n$  points  $x_1, \dots, x_n \in \mathbb{R}^d$  on the  $(d-1)$ -sphere  $S_{r_0}^{d-1}$  of radius  $r_0$ . We then vary the distance between the supports  $r_0$  to monitor the effects on the flat metric and repeat the experiment for several dimensions  $d$ . The results are depicted in [Figure 2](#). In this setting, the flat norm can be analytically computed to be

$$\rho_F(\mu, \nu) = n \min\{2, r_0\}, \quad (3.2)$$

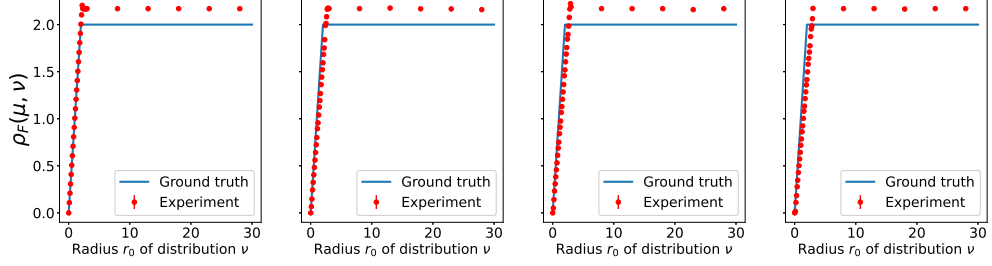


**Fig. 2** Estimates of  $\rho_F(\mu, \nu)$  over varying radii  $r_0$  and different dimensions  $d$  (from left to right:  $d = 1, d = 5, d = 10, d = 25$ ). In the  $d = 25$  case, we set  $n = 4 \times 10^4$

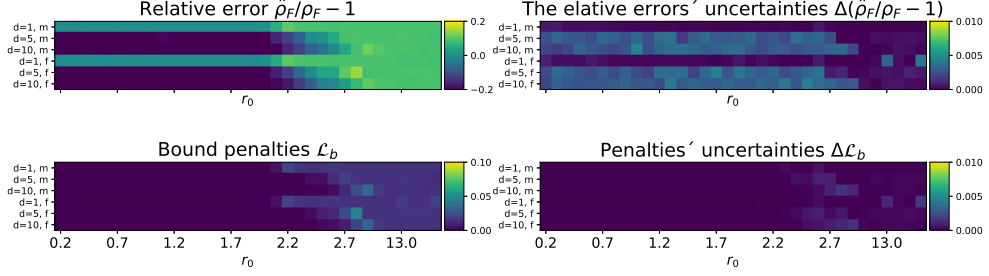


**Fig. 3** Relative errors of the estimate  $\hat{W}$  for  $\rho_F(\mu, \nu) = W$  (top left) with the corresponding final bound penalty  $\mathcal{L}_b$  (bottom left). The right column shows the corresponding uncertainties (propagated error of the change of  $\mathcal{L}_m$  over the last 50 training epochs)

independent from the dimension  $d$ . The proof of formula (3.2) is a straight forward generalization of the result (Düll et al, 2022, 1.32) and almost follows the same lines. In view of 1.3, we see that up to  $r_0 = 2$  it is more efficient to transport mass and beyond that it becomes cheaper to delete mass and create it anew.

Figure 2 shows that the estimates are very robust with respect to the considered dimensions. For radii  $r_0$  below  $\approx 2.2$  there is a slight underestimation whereas for higher  $r_0$  the distance  $\rho_F$  is systematically overestimated which stems from the bound loss  $\mathcal{L}_b$  not vanishing completely. However, the overestimation happens to the same extent for all  $r_0 \geq 2.2$  and is stable in every dimension. For a better characterization, the relative errors are depicted in Figure 3 with several dimensions,  $d = 1, 5, 10$ , and varying number of sample points, “many” ( $n = 30 \cdot 2^d$ ) vs “few” ( $n = 5 \cdot 2^d$ ). Clearly, the relative errors increase for  $r_0 \geq 2.2$  due to overestimation. Notice however, that the error is approximately homogeneous both in the number of data points as well as with respect to in the radius above the threshold. The penalties incurred to the bound are visualized in the bottom row of Figure 3. Note that for small radii the bound loss  $\mathcal{L}_b$  vanishes, as for  $r_0 \leq 2$  the 1-Lipschitz constraint ensures that the solution  $f_\Theta$  satisfies the  $\|\cdot\|_\infty$  bound in any case. For  $r_0 \geq 2.2$  one notices non-vanishing penalties as in this case mass needs to be created or deleted leading to inaccuracies. The incurred penalties are however comparable for all radii and hyperparameters. This is crucial for comparing the flat distances between several distributions.



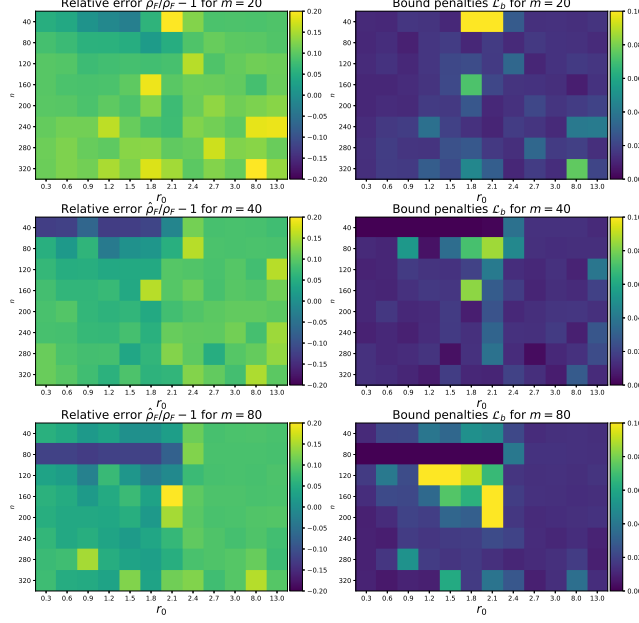


**Fig. 4** Relative errors  $\hat{\rho}_F/\rho_F - 1$  (left column) with the corresponding bound penalties  $\mathcal{L}_b$  (right column) in  $d = 2$  with few sample points

### 3.2 Testing mass differences and the effectiveness of adaptive penalties

In a next step we allow for mass differences  $n \neq m$  while keeping the distance of the base points fixed at some radius  $r_0$ , i.e.  $x_1, \dots, x_n \in S_{r_0}^{d-1}$ . In Figure 4 the relative errors as well as the incurred bound penalties are depicted for several setups. Even though there is some heterogeneity, most of the errors reside at the same order of magnitude and even around the same values. Remarkably, in the  $m = 80$  case the errors are homogeneous in all parameters for  $r_0 \geq 2$  which indicates that the deletion and creation of mass always comes at the same price. For lower  $r_0$  the error plots show stripes for  $m = n$  indicating that equal masses improve the prediction quality of the estimator.

In Figure 5 (left) the relative errors are plotted as a function of the ratio  $n/m$  confirming the stripes of uniform relative errors for equal masses  $n \approx m$ . As long as  $n/m < 6$ , i.e. the mass difference between  $\mu$  and  $\nu$  is not too dominant, the case  $r_0 > 2$  also shows homogeneous errors. This is mainly due to adaptive penalty  $\lambda$  which guarantees that the incurred errors are comparable. For comparison, the results of an analogous experiment with a fixed bound penalty  $\lambda$  are depicted in Figure 5 (middle) showing a significantly higher variance of the errors for different combinations of  $n, m, r_0$ . Without proper balance of the penalty terms, the error can hardly be controlled as soon as the mass ratio exceeds the critical threshold of  $n/m \approx 6$ . Furthermore, the histogram in Figure 6 shows the distribution of the relative errors of all considered parameter combinations either with or without an adaptive penalty. Adapting the penalty ensures

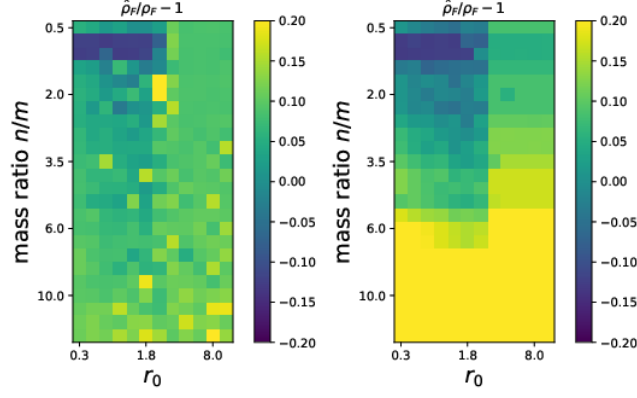


**Fig. 5** Relative errors with (left) and without adaptive penalties (right) as a function of  $r_0$  and the mass ratio  $n/m$  of both distributions. (right) Histogram of the relative error distribution with adaptive bound penalty (red) or not (blue) and bin width 0.02. The non-adaptive bound penalty was fixed to  $\lambda = 10$  and  $d = 2$  in both plots

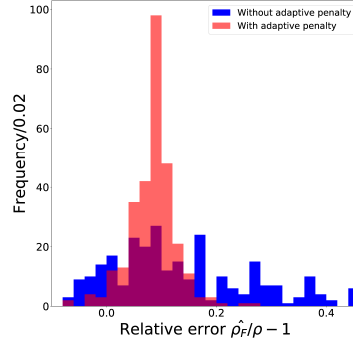


**Fig. 6** Histogram of the relative error distribution with adaptive bound penalty (red) or not (blue),  $d = 2$ , and bin width 0.02. The non-adaptive bound penalty was fixed to  $\lambda = 10$

that the distribution concentrates while simultaneously reducing the mean error from  $\hat{p}_F/\rho_F - 1 \approx 0.13$  (static case) to  $\approx 0.07$  (adaptive penalty). A repetition of the above experiments with 6 times more sample points and/or in dimension  $d = 4$  led to similar results, see Figures 10 and 11.

### 3.3 Testing unequal masses and dropping the assumptions on the support

In the last experiment supplied with analytical ground truth we drop the assumption of a fixed support and instead consider the distance between a Dirac measure located at the origin and a general linear combination of Diracs  $\nu$ . In particular, the base points  $x_1, \dots, x_n$  are now chosen arbitrarily in  $\mathbb{R}^d$  so that they differ in their distance  $d_i = \|x_i\|$

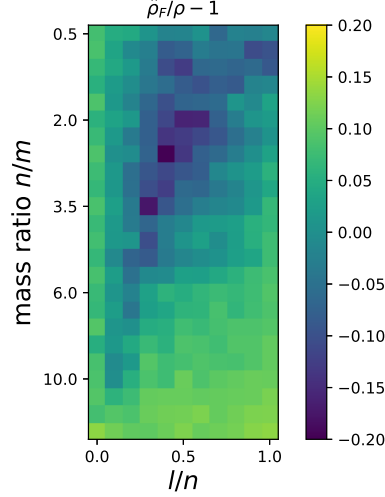


**Fig. 7** Relative errors for different parameter sets in dimension  $d = 2$ . The “creation/deletion” mode for the unbalanced optimal transport is attained for low  $l/n$  (most data points outside ball of radius 2) or high  $n/m$  (highly differing total masses of the distributions), whereas actual transport is favoured for high  $l/n$  (most data points inside ball of radius 2) or  $m/n \approx 1$ . The visible diagonal separation marks a transition between both regimes

to the origin. Consequently, the decision for mass transportation or mass creation/destruction has to be made for each individual point. Without loss of generality, the  $x_i$  are ordered with increasing distance to the origin, i.e.  $d_1 \leq d_2 \leq \dots \leq d_n$  and let  $l \in \{0, \dots, n\}$  be such that

$$\begin{cases} d_i \leq 2, & i \leq l \\ d_i > 2, & i > l \end{cases}.$$

For our experiment, we varied the total masses  $n, m$  as well as the fraction  $l/n$  which indicates which percentage of the mass for which transportation is theoretically the better strategy. For each parameter set we independently generated random data points for our distributions, computed the ground truth of  $\rho_F$  and trained the net to approximate the flat distance. The results are summarized in Figure 7. Apart from the upper triangular region bounded by  $l/n \geq 0.1$  and  $n/m \leq 6$ , the errors are comparable indicating consistent quality of our implementation for distributions with highly unbalanced masses, where mass creation/deletion is always the predominant mode. For higher ratios  $l/n$  the network has to account for both mass transportation and mass creation which only works well in the confined region defined by the visible diagonal separation. Otherwise the flat distance is underestimated in the upper region where  $m \approx l$ . In this case,  $\mu$  and  $\nu$  have roughly the same mass inside the ball  $B_2(0)$  which is the region where mass transportation is more efficient. Theoretically, in this case all the mass inside  $B_2(0)$  should be transported and all mass outside deleted. As it seems, the algorithm tends to underestimate mass transportation and to overestimate

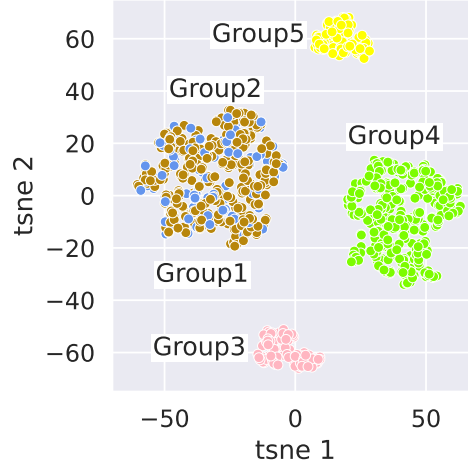


**Fig. 8** 2D t-SNE plot of mRNA counts for 5 distributions generated by *Splatter*

mass deletion. A similar experiment in  $d = 4$  with more data points yielded similar results with only minor qualitative differences.

### 3.4 Toy Experiment: High dimensional simulated data

In a second step, we analyzed high dimensional simulated single-cell (sc) transcriptomics data generated by the *R*-software package *Splatter*. It was developed by Zappia et al. [Zappia et al \(2017\)](#) to generate simulated scRNA sequencing count data of differentiation trajectories or of populations with one or multiple cell types. The simulation is based on a Gamma-Poisson distribution which models the expression levels of genes within cells as well as effects such as differing library sizes or dropouts. We refer to our Github repository for a simulation script and a comprehensive workflow of the analysis. While there is no analytical ground truth available in this setting, we still have the possibility to monitor qualitative changes of the implementation via appropriate parameter choices in the *Splatter* framework. In particular, we modelled five different cell groups by varying the sample size and the genetic expression profile, i.e. the location in gene space. After preprocessing and reducing the generated data to 5 dimensions, we determined the flat distances between the individual groups, see [Table 1](#). For comparison, we compute the corresponding Wasserstein distances of the separately normalized distributions as well.

One clearly notices the systematic differences between the flat metric and the Wasserstein distance. As the latter is insensitive to population size, distributions 1 (blue) and 2 (brown) are nearly identical in Wasserstein space whereas they are clearly distinguishable with respect to the flat metric due to the large mass difference. Taking the mass into account significantly influences the neighbouring relation of the groups. The same conclusions hold in a high-dimensional setting as well, cf. [Appendix B.4](#). Thus, if differences in cluster sizes are not only an effect of sampling but rather play a relevant

**Table 1** Flat distances (first entry of each cell) between the clusters. For comparison the respective Wasserstein distances using the same net architecture are displayed (second entry of each cell)

	Group 1	Group 2	Group 3	Group 4	Group 5
Group 1	(0.00, 0.00)	(2.61, 0.24)	(2.26, 7.21)	(4.70, 7.22)	(2.28, 9.94)
Group 2	(2.63, 0.25)	(0.00, 0.00)	(5.03, 7.23)	(2.17, 7.23)	(5.07, 9.95)
Group 3	(2.27, 7.19)	(5.03, 7.23)	(0.00, 0.00)	(5.04, 10.26)	(2.18, 12.14)
Group 4	(4.70, 7.17)	(2.17, 7.24)	(5.04, 10.25)	(0.00, 0.00)	(5.09, 11.99)
Group 5	(2.28, 9.94)	(5.07, 9.93)	(2.18, 12.18)	(5.09, 12.06)	(0.00, 0.00)

role for the underlying question, we highly recommend using a method for unnormalized data distributions. Notice however, that the distances displayed in Table 1 - both with respect to the flat metric and the Wasserstein distance - are only ordinal and not cardinal.

## 4 Conclusion

In this paper, we introduced an implementation of the flat metric  $\rho_F$  for nonnegative Radon measures without a mass restriction. Particular focus was put on comparability of pairwise computed distances from independently trained networks. The combination of architectural (spectral normalization, GroupSort activation function) and regularization constraints (bound penalty loss  $\mathcal{L}_b$ ) turned out to be effective for estimating the flat distance as shown in several experiments. Throughout the tests varying the hyperparameters – both of the network architecture as well as of the analyzed problems – did not yield qualitative discrepancies of the output indicating that the default setup of the net is robust. Choosing the enforcing parameter adaptively considerably shrunk the fluctuations in the relative errors guaranteeing that pairwise comparisons of distributions are possible. We remark that our results will usually be biased towards too high values, so that ordering of input distributions with respect to our implementation is rather ordinal than cardinal.

In contrast to the Wasserstein distance, our solution was capable of taking the effects of varying population sizes into account when comparing several data distributions. These results indicate that our estimator for the flat distances qualitatively exhibits the expected behaviour and can be used to estimate distances of real life data.

**Supplementary information.**

## **Declarations**

### **Funding**

The authors did not receive support from any organization for the submitted work.

### **Ethics approval**

Not applicable

### **Consent**

Not applicable

### **Availability of data and materials**

Not applicable

### **Code availability**

The code is available at [https://github.com/hs42/flat\\_metric](https://github.com/hs42/flat_metric)

### **Author contribution statement**

Both authors contributed equally to this research. The idea for this paper is based on the thesis of Henri Schmidt at Heidelberg University.

## **Appendix A Methods**

The bound loss enforcing parameter  $\lambda$  is updated during runtime. This is done to ensure that different networks solve the same optimization problem and that hence their outcomes are comparable to one another. Notably, updates occur at fractions  $s_1 = 0.2$ ,  $s_2 = 0.5$ , and  $s_3 = 0.8$  of all training epochs. Initially,  $\lambda$  is set to an initial value  $\lambda_{init} = 10$ . The net is then trained until  $s_1$  and we set  $\lambda_{s_1} = -2\mathcal{L}_m$ , i.e. to twice the current estimate for the flat distance. Thus, at  $s_1$  we adapt the scale of  $\mathcal{L}_b$  according to  $\mathcal{L}_m$ . If the flat distance loss is high, so should be the penalty loss and both contributions are balanced to the same ratio. After  $s_2$ , we instead look directly at the bound penalty  $\mathcal{L}_b$  as we are interested in how much  $f_\Theta$  exceeds the bound  $M$ . The actual penalty is compared to a target value of  $b_t = 0.02$ , i.e. we encourage each net  $f_\Theta$  to disregard the boundedness constraint to the same extent by setting  $\lambda$  to  $\lambda_{s_2} = \lambda_{s_1} \frac{\mathcal{L}_b}{b_t}$ . During the corresponding training epochs,  $\lambda = \lambda(t)$  interpolates linearly between the target values  $\lambda_{s_1}, \lambda_{s_2}$  and  $\lambda_{s_3}$ . After  $s_3$ ,  $\lambda(t)$  remains constant.

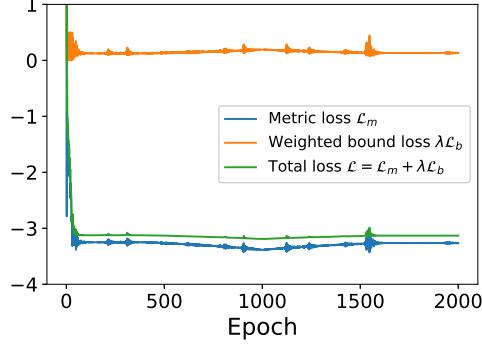


**Fig. 9** Loss terms during training of the experiment with  $r_0 = 28$  and  $d = 2$

In summary, we have

$$\lambda(t) = \begin{cases} \lambda_{init} & 0 \leq t < s_1 \\ \frac{\lambda_{init} - \lambda_{s_1}}{s_2 - s_1}(t - s_2) + \lambda_{init} & s_1 \leq t < s_2 \\ \frac{\lambda_{s_1} - \lambda_{s_2}}{s_3 - s_2}(t - s_3) + \lambda_{s_1} & s_2 \leq t < s_3 \\ \lambda_{s_2} & s_3 \leq t \leq 1 \end{cases} \quad (\text{A1})$$

## Appendix B Experimental Details

### B.1 Toy experiment: The distance of the supports

In our first experiment we show that, as in the Wasserstein case, the distance between the supports of the measures plays an important role. To this end, we eliminate the effect of the mass difference by considering measures with the same total variation norm  $n \in \mathbb{N}$ . One measure is fixed at the origin, i.e.  $\mu = n\delta_0$ , whereas for the other one we randomly sample  $n$  points  $x_1, \dots, x_n \in \mathbb{R}^d$  on the  $(d-1)$ -sphere  $S_{r_0}^{d-1}$  of radius  $r_0$ , and consider their linear combination  $\nu = \sum_{i=1}^n \delta_{x_i}$ .

In practice,  $\mu, \nu$  are constructed as empiric measures by drawing  $n$  changing random vectors located at the origin or at  $S_{r_0}^{d-1}$  respectively. To account for the increase in surface area with the dimension  $d$  we couple the sample size to  $d$ . Specifically, we set  $n := 30 \cdot 2^d$  in order to approximate  $\mu, \nu$  well. The radii probed are  $r_0 \in \{0.01, 0.11, 0.21, \dots, 2.91, 3, 8, 13, 18, 23, 28\}$ . For each  $r_0$  and each  $d$  we train a new neural network for 2000 epochs, where we chose two hidden layers of 128 neurons each as an architecture. The flat distance is extracted as the mean of  $-\mathcal{L}_m$  over the last 50 training epochs with the corresponding error of the mean  $\sigma/\sqrt{50}$ . Note that for  $d = 25$  a lower value for the number of samples than the usual  $n = 30 \cdot 2^d$  was chosen in order to be feasible to compute. The results are depicted in Figure 2.

In Figure 9 we examined the mutual interactions of both loss terms. As can be seen both contributions act antagonistically as evident from the synchronous ripples and the dents around epoch 1000: Optimizing  $\mathcal{L}_m$  first incurs at a cost on  $\mathcal{L}_b$  and is then balanced by joint minimization of both constraints.

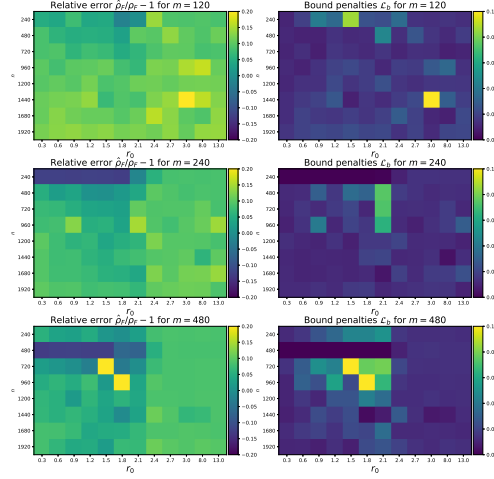


**Fig. 10** Relative errors and bound penalties in  $d = 2$  dimensions in dependency of  $r_0$ ,  $n = \alpha\tilde{n}$ , and  $m = \alpha\tilde{m}$ .  $\alpha$  was set to the “many samples” setting  $\alpha = 6 \cdot 2^d$

## B.2 Testing mass differences and the effectiveness of adaptive penalties

In the second experiment we vary the mass between both measures but still control for the distance of the supports. For simplicity, we invoke the scale invariance of the flat metric and scale both measures with the lower mass such that at least one measure is normalized. In particular, we consider total masses  $n, m \in \mathbb{N}$  and measures

$$\mu = \frac{m}{\min\{m, n\}} \delta_0 \quad \text{and} \quad \nu = \frac{1}{\min\{m, n\}} \sum_{i=1}^n \delta_{x_i}$$

for points  $x_1, \dots, x_n \in S_{r_0}^{d-1}$ . In practice, we will set  $n = \alpha\tilde{n}$ ,  $m = \alpha\tilde{m}$  where  $\alpha = 2^d$  is a factor to account for the increase in surface area in higher dimensions which leads to the need for more data points. Adjusting the more general formula presented in Proposition 1 to this setting, the ground truth for the flat distance is given by

$$\rho_F(\mu, \nu) = \min\{2, r_0\} + \frac{1}{\min\{m, n\}} |n - m|. \quad (\text{B1})$$

The relative errors as well as the incurred bound penalties are depicted in Figure 4. Each row comprises a new value for  $\tilde{m}$ , while  $\tilde{n}$  is varied on the respective y-axis and  $r_0$  on the x-axis. The parameters tested were  $\tilde{m} \in \{5, 10, 20\}$ ,  $\tilde{n} \in \{10, \dots, 80\}$ . The dimension was set to  $d = 2$  so that  $\alpha = 4$ . We repeated the experiment with six times more data points, i.e.  $\alpha = 6 \cdot 2^d$ , and in dimension  $d = 4$  with comparable outcome, see Figure 10 and Figure 11 respectively.



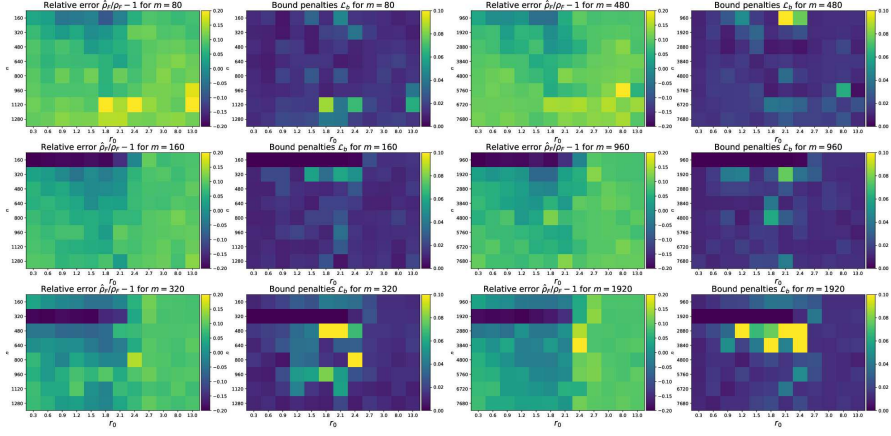


**Fig. 11** Relative errors and bound penalties in  $d = 4$  with few sample points (left;  $\alpha = 2^d$ ) and many sample points (right;  $\alpha = 6 \cdot 2^d$ )

### B.3 Testing unequal masses and dropping the assumptions on the support

In a last step, we consider the distance between a Dirac measure located at the origin and a general linear combination of Diracs  $\nu$ . As before, we scale both measures by the factor  $1/\min\{m, n\}$  such that at least one measure is a probability measure which leads to

$$\mu = \frac{m}{\min\{m, n\}} \delta_0, \quad \text{and} \quad \nu = \frac{1}{\min\{m, n\}} \sum_{i=1}^n \delta_{x_i},$$

with arbitrary points  $x_i \in \mathbb{R}^d$ . Without loss of generality, the  $x_i$  are ordered with increasing distance to the origin, i.e.  $d_1 \leq d_2 \leq \dots \leq d_n$  and let  $l \in \{0, \dots, n\}$  be such that

$$\begin{cases} d_i \leq 2, & i \leq l \\ d_i > 2, & i > l \end{cases}.$$

In view of Equation (B1) the parameter  $l$  denotes the part of  $\nu$  for which mass transportation is theoretically more efficient. According to Proposition 1, the flat distance between  $\mu$  and  $\nu$  is given by

$$\rho_F(\mu, \nu) = \frac{1}{\min\{n, m\}} \left( |m - l| + n - l + \sum_{i=1}^{\lfloor \lambda \rfloor} d_i + (\lambda - \lfloor \lambda \rfloor) d_{\lfloor \lambda \rfloor + 1} \right), \quad (\text{B2})$$

where  $\lambda = \min\{l, m\}$  and  $\lfloor \cdot \rfloor$  denotes the usual floor function.

In practice, we uniformly sampled  $\mathcal{O}(10^2)$  points  $x_1, \dots, x_n$  in an open ball  $B_{200}(0) \subset \mathbb{R}^d$  under the restriction that  $l$  of them actually reside within  $B_2(0) \subset \mathbb{R}^d$ . To prevent

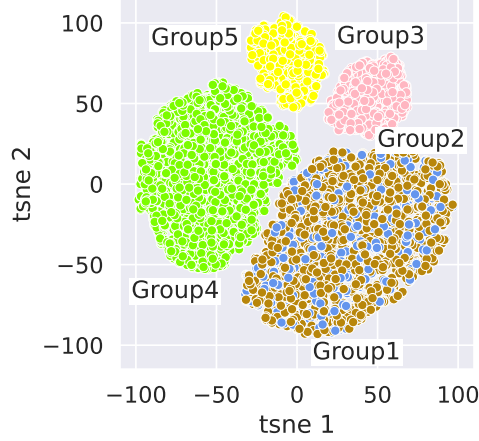


**Fig. 12** 2D t-SNE plot of mRNA counts for 5 distributions generated by *Splatter*. The only difference to Figure 8 is that population sizes were increased by a factor of 10

overfitting of our network, we reduced the linear layers to 64 neurons in both hidden layers and increased the number of training epochs to 10000.

## B.4 Splatter

We first simulate the mRNA counts of a batch consisting 1000 cells, each expressing 5000 genes. These cells were divided into five distinct groups of expression profiles. By modifying the *de.prob* parameter group three and four have been constructed to express more distinct genes compared to the reference expression profile and even more so for group five. On the other hand, group one and two were set to have similar expressed genes leading to an overlap in gene space. Furthermore, groups one, three, and five had 3.5 times less cells than group two and four. Thus, we can observe the influence of the mass differences as well as the spread of the distributions on the flat metric.

The generated “raw” data was preprocessed in a standard way by filtering out highly variable genes, normalizing the data to the library size and centering. Lastly, a principal component analysis (PCA) selected the 5 most important dimensions which were then further reduced to 2 for visualization in a t-SNE plot (cf. Figure 8). To show that our solution works for arbitrary dimensions (save for the curse of dimensionality), we reduced the Splatter data also to 50 instead of 5 features and performed the same analysis. In doing so, we generated new data with the same parameters but for 10000 cells rather than 1000. The conclusions are similar as for the low-dimensional case as can be seen from the results below:

## B.5 Architectural hyperparameters

Lastly, we examine the influence of the architectural hyperparameters on the performance of the neural network by repeating the experiment described in Section B.2.

**Table 2** Flat distances (first entry of each cell) between the clusters for dimension 50. For comparison the respective Wasserstein distances using the same net architecture are displayed (second entry of each cell)

	Group 1	Group 2	Group 3	Group 4	Group 5
Group 1	(0.00, 0.00)	(3.15, 0.35)	(2.17, 6.77)	(5.15, 6.85)	(2.25, 9.75)
Group 2	(3.16, 0.35)	(0.00, 0.00)	(5.16, 6.76)	(2.16, 6.85)	(4.79, 9.76)
Group 3	(2.17, 6.77)	(5.15, 6.76)	(0.00, 0.00)	(5.21, 9.51)	(2.26, 11.86)
Group 4	(5.15, 6.85)	(2.16, 6.68)	(5.20, 9.51)	(0.00, 0.00)	(4.83, 12.05)
Group 5	(2.25, 9.75)	(4.79, 9.76)	(2.27, 11.86)	(4.84, 12.05)	(0.00, 0.00)

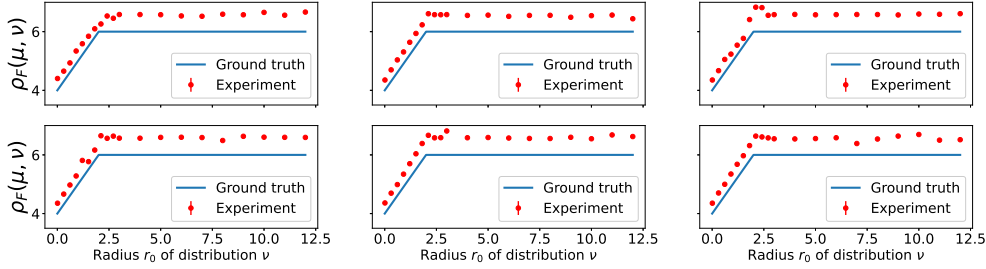


**Fig. 13** Showcases of different architectural hyperparameters. From left to right, top to bottom: SN with two hidden layers à 128 neurons and bundles of 2; BO with two hidden layers à 128 neurons and bundles of 2; SN with five hidden layers à 128 neurons and bundles of 2; SN with two hidden layers à 512 neurons and bundles of 8; BO with five hidden layers à 128 neurons and bundles of 2; BO with two hidden layers à 512 neurons and bundles of 8

Specifically, we considered the measures

$$\mu = \frac{m}{\min\{m, n\}} \delta_0 \quad \text{and} \quad \nu = \frac{1}{\min\{m, n\}} \sum_{i=1}^n \delta_{x_i}$$

for points  $x_1, \dots, x_n \in S_{r_0}^{d-1}$  with  $n = 2^4 \times 50$ ,  $m = 2^4 \times 10$  and  $d = 4$  and observed the qualitative change of the estimates with  $r_0$ . We both considered spectral normalization (SN) and Björck orthonormalization (BO) and changed the number of layers and the grouping size of Groupsort; each time 10000 training epochs were used. The results are shown in Figure 13 where the top left depicts our control setup used in the other parts of this paper. While there are naturally quantitative differences, Figure 13 shows that there are no qualitative differences and no analyzed cases is obviously better suited to make predictions, i.e. is closer to the ground truth. A possible expectation is that of Björck orthonormalization with large hidden layers and bundles of 8 (bottom right), which shows some unexpected oscillations. We conclude that our usual architectural setup is suited for this specific and for similar tasks.

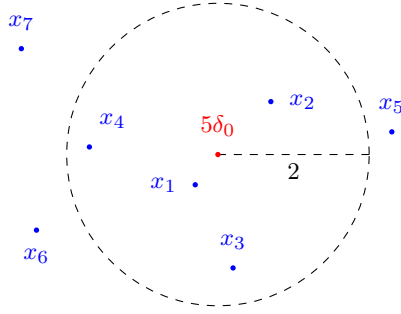


**Fig. 14** Illustration of the first example:  $c = 5, l = 4, n = 7, \lambda = 4$

## Appendix C Analytical Ground Truth

**Proposition 1.** Let  $n \in \mathbb{N}$  and  $c \in \mathbb{R}^+$ . Consider points  $x_0, x_1, \dots, x_n \in \mathbb{R}^d$  which are ordered with increasing distance to  $x_0$ , i.e. for  $d_i := |x_0 - x_i|$  we have  $d_1 \leq d_2 \leq \dots \leq d_n$  and let  $l \in \{0, \dots, n\}$  be such that

$$\begin{cases} d_i \leq 2, & i \leq l, \\ d_i > 2, & i > l \end{cases}.$$

Define  $\lambda = \min\{c, l\}$ . Then the flat distance between the measures  $\mu = c\delta_{x_0}$  and  $\nu = \sum_{i=1}^n \delta_{x_i}$  is given by

$$\rho_F(\mu, \nu) = |c - l| + n - l + \sum_{i=1}^{\lfloor \lambda \rfloor} d_i + (\lambda - \lfloor \lambda \rfloor)d_{\lfloor \lambda \rfloor + 1}, \quad (\text{C1})$$

where  $\lfloor \cdot \rfloor$  denotes the usual floor function.

To clarify formula (C1) we provide two examples.

**Example 1.** • Let  $\mu = 5\delta_0$  and  $\nu = \sum_{i=1}^7 \delta_{x_i}$ , where  $d_i < 2$  for  $i = 1, \dots, 4$  and  $d_i > 2$  for  $i = 5, 6, 7$ . See Figure 14. Then formula (C1) reads

$$\rho_F(\mu, \nu) = |5 - 4| + 7 - 4 + \sum_{i=1}^4 d_i = 4 + \sum_{i=1}^4 d_i.$$

• Let  $\mu = 2.5\delta_0$  and  $\nu = \sum_{i=1}^4 \delta_{x_i}$ , where  $d_i < 2$  for  $i = 1, 2, 3$  and  $d_4 > 2$ . See Figure 15. Then formula (C1) yields

$$\rho_F(\mu, \nu) = |3 - 2.5| + 4 - 3 + \sum_{i=1}^2 d_i + (2.5 - 2)d_3.$$

*Proof.* We apply the alternative characterisation of Piccoli and Rossi (1.3) and consequently have to find the optimal submeasures  $\tilde{\mu}, \tilde{\nu}$ . As  $\mu$  is a Dirac measure located at

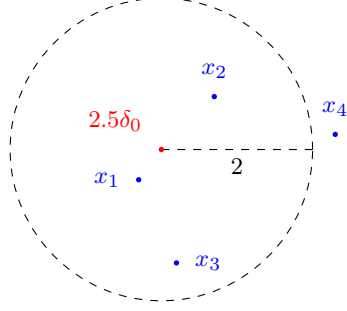


**Fig. 15** Illustration of the second example:  $c = 2.5$ ,  $l = 3$ ,  $n = 4$ ,  $\lambda = 2.5$

$x_0$ , any submeasure of  $\mu$  is of the form  $\tilde{\mu}_\alpha = \alpha\delta_{x_0}$  for some  $\alpha \in [0, c]$ . The parameter  $\alpha$  consequently denotes the share of the mass located at  $x_0$  which we want to transport to  $\nu$ . We can thus compute directly

$$\|\mu - \tilde{\mu}_\alpha\|_{TV} = (c - \alpha)\|\delta_{x_0}\|_{TV} = c - \alpha. \quad (\text{C2})$$

The case for submeasures of  $\nu$  is slightly more difficult as  $\nu$  is a linear combination of Diracs. However, any  $\tilde{\nu}$  is definitely of the form  $\tilde{\nu}_{\alpha,\beta} = \sum_{i=1}^n \beta_i \delta_{x_i}$  with weights  $\beta_i \in [0, 1]$  satisfying  $\sum_{i=1}^n \beta_i = \alpha$  as both submeasures need to have the same total mass. The weights  $\beta_i$  indicate how much of the mass located at  $x_i$  comes via transportation from  $x_0$ , whereas the rest  $1 - \beta_i$  has to be created. We compute

$$\|\nu - \tilde{\nu}_{\alpha,\beta}\|_{TV} = \left\| \sum_{i=1}^n (1 - \beta_i) \delta_{x_i} \right\|_{TV} = \sum_{i=1}^n (1 - \beta_i) \|\delta_{x_i}\|_{TV} = \sum_{i=1}^n (1 - \beta_i) = n - \alpha, \quad (\text{C3})$$

where we used that the total variation norm behaves linearly for nonnegative measures. What is left to check is the Wasserstein distance between  $\tilde{\mu}_\alpha$  and  $\tilde{\nu}_{\alpha,\beta}$ . If  $\alpha = 0$ , then clearly  $W_1(\tilde{\mu}_\alpha, \tilde{\nu}_{\alpha,\beta}) = 0$ , so let  $\alpha > 0$  for the upcoming computation

$$W_1(\tilde{\mu}_\alpha, \tilde{\nu}_{\alpha,\beta}) = W_1\left(\alpha\delta_{x_0}, \sum_{i=1}^n \beta_i \delta_{x_i}\right) = \int_{\mathbb{R}^d} |x_0 - y| \, d\left[\sum_{i=1}^n \beta_i \delta_{x_i}\right](y) = \sum_{i=1}^n \beta_i |x_0 - x_i|. \quad (\text{C4})$$

Here we used that the Wasserstein distance between a Dirac measure and an arbitrary probability measure  $\eta$  is given by

$$W_1(\eta, \delta_{x_0}) = \int_{\mathbb{R}^d} |x_0 - y| \, d\eta(y).$$

In view of identity (1.3) we combine (C2), (C3) and (C4) to get the following estimate

$$\begin{aligned}\rho_F(\mu, \nu) &\leq \|\mu - \tilde{\mu}_\alpha\|_{TV} + \|\nu - \tilde{\nu}_{\alpha, \beta}\|_{TV} + W_1(\tilde{\mu}_\alpha, \tilde{\nu}_{\alpha, \beta}) \\ &= c + n - 2\alpha + \sum_{i=1}^n \beta_i d_i =: F(\alpha, \beta),\end{aligned}\tag{C5}$$

with  $\alpha = \sum_{i=1}^n \beta_i$  so that the case  $\alpha = 0$  is included. As all possible submeasures are of the form  $\tilde{\mu}_\alpha, \tilde{\nu}_{\alpha, \beta}$  we reduced the problem to minimizing  $F$  subject to the constraint  $\alpha = \sum_{i=1}^n \beta_i$ . We claim that the global minimum is attained in  $(\alpha^*, \beta^*)$  where

$$\alpha^* = \min\{l, c\} \quad \text{and} \quad \beta_i^* = \begin{cases} 1, & i \leq \lfloor \alpha^* \rfloor, \\ \alpha^* - \lfloor \alpha^* \rfloor, & i = \lfloor \alpha^* \rfloor + 1, \\ 0, & \text{else.} \end{cases}\tag{C6}$$

In Remark 1 we give a short heuristic for this specific parameter choice. Before we prove the optimality, we show that (C6) leads to (C1). So we plug in  $(\alpha^*, \beta^*)$  into  $F$  and treat both cases of  $\alpha^*$  separately.

Case 1:  $l \leq c$

In this case  $\alpha^* = l \in \mathbb{N}$ , so that  $\lfloor \alpha^* \rfloor = \alpha^*$  and thus

$$F(l, \beta^*) = c + n + \sum_{i=1}^l (d_i - 2) = c + n - 2l + \sum_{i=1}^l d_i = |c - l| + n - l + \sum_{i=1}^l d_i.$$

Case 2:  $c \leq l$

In this case  $\alpha^* = c \in \mathbb{R}^+$ , so that

$$\begin{aligned}F(c, \beta^*) &= c + n + \sum_{i=1}^{\lfloor c \rfloor} (d_i - 2) + (c - \lfloor c \rfloor)(d_{\lfloor c \rfloor + 1} - 2) \\ &= c + n + \sum_{i=1}^{\lfloor c \rfloor} d_i - 2\lfloor c \rfloor + (c - \lfloor c \rfloor)d_{\lfloor c \rfloor + 1} - 2c + 2\lfloor c \rfloor \\ &= |c - l| + n - l + \sum_{i=1}^{\lfloor c \rfloor} d_i + (c - \lfloor c \rfloor)d_{\lfloor c \rfloor + 1}\end{aligned}$$

as desired.

We are left to prove that  $(\alpha^*, \beta^*)$  yields the global minimum of  $F$ . To show this, we invoke variational inequality theory. First note that the domain of  $F$

$$X := \left\{ (\alpha, \beta) \in [0, c] \times [0, 1]^n \mid \alpha - \sum_{i=1}^n \beta_i = 0 \right\}$$

is nonempty, closed and convex. Furthermore,  $F : X \rightarrow \mathbb{R}$  is smooth, linear and thus convex. Let  $x^* := (\alpha^*, \beta^*)$ . According to (Geiger and Kanzow, 2002, Lemma 7.5) the point  $x^*$  is a global minimum of  $F$  if  $x^*$  solves the variational inequality

$$VIP(X, \nabla F) := \nabla F(x^*)^T(x - x^*) \geq 0 \quad \forall x \in X. \quad (\text{C7})$$

We compute for some  $x = (\alpha, \beta) \in X$

$$\begin{aligned} \nabla F(x^*)^T(x - x^*) &= \begin{pmatrix} -2 \\ d_1 \\ \vdots \\ d_n \end{pmatrix}^T \begin{pmatrix} \alpha - \alpha^* \\ \beta_1 - \beta_1^* \\ \vdots \\ \beta_n - \beta_n^* \end{pmatrix} = -2(\alpha - \alpha^*) + \sum_{i=1}^n d_i(\beta_i - \beta_i^*) \\ &= -2 \left( \sum_{i=1}^n \beta_i - \sum_{i=1}^n \beta_i^* \right) + \sum_{i=1}^n d_i(\beta_i - \beta_i^*) = \sum_{i=1}^n (d_i - 2)(\beta_i - \beta_i^*). \end{aligned}$$

Plugging in  $\beta^*$  yields

$$\begin{aligned} &\nabla F(x^*)^T(x - x^*) \\ &= \sum_{i=1}^{\lfloor \alpha^* \rfloor} (d_i - 2)(\beta_i - 1) + (d_{\lfloor \alpha^* \rfloor + 1} - 2)(\beta_{\lfloor \alpha^* \rfloor + 1} - \alpha^* + \lfloor \alpha^* \rfloor) + \sum_{i=\lfloor \alpha^* \rfloor + 2}^n (d_i - 2)\beta_i. \end{aligned} \quad (\text{C8})$$

To see that (C8) is actually nonnegative for all  $x \in X$  we have to distinguish cases for  $\alpha^*$ .

Case 1:  $\alpha^* = l$

Then  $\alpha^* = \lfloor \alpha^* \rfloor$  and (C8) reads

$$\nabla F(x^*)^T(x - x^*) = \sum_{i=1}^l \underbrace{(d_i - 2)}_{\leq 0} \underbrace{(\beta_i - 1)}_{\leq 0} + \sum_{i=l+1}^n \underbrace{(d_i - 2)}_{> 0} \beta_i \geq 0 \quad \forall (\alpha, \beta) \in X.$$

In particular,  $x^*$  solves the variational inequality (C7) and is thus the global minimum of  $F$ .

Case 2:  $\alpha^* = c < l$

Then  $\lfloor c \rfloor + 1 \leq l$  and (C8) reads

$$\begin{aligned}
& \nabla F(x^*)^T(x - x^*) \\
&= \sum_{i=1}^{\lfloor c \rfloor} (d_i - 2)(\beta_i - 1) + (d_{\lfloor c \rfloor + 1} - 2)(\beta_{\lfloor c \rfloor + 1} - c + \lfloor c \rfloor) + \sum_{i=\lfloor c \rfloor + 2}^n (d_i - 2)\beta_i \\
&= \sum_{i=1}^{\lfloor c \rfloor} (d_i - 2)(\beta_i - 1) + (d_{\lfloor c \rfloor + 1} - 2)(\beta_{\lfloor c \rfloor + 1} - c + \lfloor c \rfloor) + \sum_{i=\lfloor c \rfloor + 2}^l (d_i - 2)\beta_i + \sum_{i=l+1}^n (d_i - 2)\beta_i.
\end{aligned} \tag{C9}$$

In this case bounding the right-hand side from below is not as the  $\beta_i$  are linked together via the constraint  $\sum_{i=1}^n \beta_i = \alpha$ . Nevertheless, the last term is nonnegative for all  $\beta \in X$ , whereas all the terms in the first three terms of the sum are monotonically decreasing in  $\beta_i$  and  $\beta_{\lfloor c \rfloor + 1}$ , respectively. Consequently, we set  $\beta_i = 0$  for  $i > l$  which yields

$$\begin{aligned}
& \nabla F(x^*)^T(x - x^*) \\
&\geq \sum_{i=1}^{\lfloor c \rfloor} (d_i - 2)(\beta_i - 1) + (d_{\lfloor c \rfloor + 1} - 2)(\beta_{\lfloor c \rfloor + 1} - c + \lfloor c \rfloor) + \sum_{i=\lfloor c \rfloor + 2}^l (d_i - 2)\beta_i \\
&= \sum_{i=1}^{\lfloor c \rfloor} d_i(\beta_i - 1) + d_{\lfloor c \rfloor + 1}(\beta_{\lfloor c \rfloor + 1} - c + \lfloor c \rfloor) + \sum_{i=\lfloor c \rfloor + 2}^l d_i\beta_i - 2 \sum_{i=1}^l \beta_i + 2\lfloor c \rfloor + 2c - 2\lfloor c \rfloor \\
&= \sum_{i=1}^{\lfloor c \rfloor} d_i(\beta_i - 1) + d_{\lfloor c \rfloor + 1}(\beta_{\lfloor c \rfloor + 1} - c + \lfloor c \rfloor) + \sum_{i=\lfloor c \rfloor + 2}^l d_i\beta_i + 2(c - \alpha),
\end{aligned}$$

where we used the improved constraint  $\sum_{i=1}^l \beta_i = \alpha$ . Using the constraint again gives

$$\begin{aligned}
& \nabla F(x^*)^T(x - x^*) \\
&\geq \sum_{i=1}^{\lfloor c \rfloor} d_i(\beta_i - 1) + d_{\lfloor c \rfloor + 1} \left( \alpha - \sum_{i=1}^{\lfloor c \rfloor} \beta_i - \sum_{i=\lfloor c \rfloor + 2}^l \beta_i - c + \lfloor c \rfloor \right) + \sum_{i=\lfloor c \rfloor + 2}^l d_i\beta_i + 2(c - \alpha) \\
&= \sum_{i=1}^{\lfloor c \rfloor} d_i(\beta_i - 1) + d_{\lfloor c \rfloor + 1} \left( \sum_{i=1}^{\lfloor c \rfloor} (1 - \beta_i) \right) + \sum_{i=\lfloor c \rfloor + 2}^l (d_i - d_{\lfloor c \rfloor + 1})\beta_i + (2 - d_{\lfloor c \rfloor + 1})(c - \alpha) \\
&= \sum_{i=1}^{\lfloor c \rfloor} \underbrace{(d_{\lfloor c \rfloor + 1} - d_i)}_{\geq 0} \underbrace{(1 - \beta_i)}_{\geq 0} + \sum_{i=\lfloor c \rfloor + 2}^l \underbrace{(d_i - d_{\lfloor c \rfloor + 1})}_{\geq 0} \beta_i + \underbrace{(2 - d_{\lfloor c \rfloor + 1})}_{\geq 0} \underbrace{(c - \alpha)}_{\geq 0} \geq 0.
\end{aligned} \tag{C10}$$



Note that we used once more that  $c < l$  implies  $\lfloor c \rfloor + 1 \leq l$ , so that  $d_{\lfloor c \rfloor + 1} \leq 2$ . From (C10) we conclude that  $x^*$  solves the variational inequality (C7) also in the case  $\alpha^* = c$  and  $x^*$  is thus the global minimum of  $F$ .  $\square$

**Remark 1.** Now we give a short heuristic for the optimal choice  $(\alpha^*, \beta^*)$  given in (C6). In a first step, we fix the amount of mass  $\alpha$  that we want to transport and look for the optimal weights  $\beta$  given  $\alpha$ . Clearly,  $\beta_i = 0$  for all  $i = 1, \dots, n$  if  $\alpha = 0$ , so we will consider  $\alpha > 0$  now. According to (C5) we have the estimate

$$\rho_F(\mu, \nu) \leq c + n - 2\alpha + \sum_{i=1}^n \beta_i d_i. \quad (\text{C11})$$

It is clearly optimal to transport as much mass as shortly as possible. As the  $d_i$  are ordered increasingly, this means that we prioritize the lower indices over higher ones. In particular, we assign the maximal value of 1 to the first  $\lfloor \alpha \rfloor$  entries of  $\beta$ . The remaining mass  $\alpha - \lfloor \alpha \rfloor$  is then assigned to the next entry, i.e. to  $\beta_{\lfloor \alpha \rfloor + 1}$ . All other entries are set to zero, so that this scheme yields the following weight vector  $\beta^* = \beta^*(\alpha)$ :

$$\beta_i^* = \begin{cases} 1, & i \leq \lfloor \alpha \rfloor, \\ \alpha - \lfloor \alpha \rfloor, & i = \lfloor \alpha \rfloor + 1, \\ 0, & \text{else.} \end{cases} \quad (\text{C12})$$

We note that distributing the mass in any other way by choosing different  $\beta_i$  can not yield a better overall transportation cost  $W_1(\tilde{\mu}_\alpha, \nu_{\alpha, \beta})$  as we would potentially transport more mass to locations further away at the expense of nearer locations. However, equally efficient transport plans might be possible if there are points with the same distance to  $x_0$  so that mass transportation is indifferent between those locations. Now we are left to find the optimal choice of  $\alpha$  which minimizes (C11). So we define

$$\begin{aligned} \tilde{F}(\alpha) &:= F(\alpha, \beta^*) = c + n - 2\alpha + \sum_{i=1}^{\lfloor \alpha \rfloor} d_i + (\alpha - \lfloor \alpha \rfloor) d_{\lfloor \alpha \rfloor + 1} \\ &= c + n + \sum_{i=1}^{\lfloor \alpha \rfloor} (d_i - 2) + (\alpha - \lfloor \alpha \rfloor)(d_{\lfloor \alpha \rfloor + 1} - 2). \end{aligned} \quad (\text{C13})$$

We first note that  $d_i - 2 \leq 0$  for all  $i \leq l$ , so that  $\tilde{F}(\alpha)$  is monotonically decreasing for  $\alpha \leq l$ . In particular, choosing  $\alpha > l$  can not be optimal as it would add positive terms to (C13) which is clearly not minimal. Since  $\alpha$  is still bounded by  $c$  we conclude the bound  $\alpha \leq \min\{l, c\}$  which will be exactly attained in the optimum (i.e.  $\alpha^* = \min\{l, c\}$ ) due to monotonicity of  $F$ .

It is important to note that this approach just provides a heuristic for the global minimum  $(\alpha^*, \beta^*)$  and that a proof for the optimality is still necessary. In this Remark we

computed

$$\min_{\alpha} \min_{\beta} F(\alpha, \beta) \quad \text{instead of} \quad \min_{\alpha, \beta} F(\alpha, \beta)$$

under the constraint  $\sum_{i=1}^n \beta_i = \alpha$ . In general, the second term is smaller than the first.

## References

- Anil C, Lucas J, Grosse R (2019) Sorting out Lipschitz function approximation. In: Chaudhuri K, Salakhutdinov R (eds) Proceedings of the 36th International Conference on Machine Learning, Proceedings of Machine Learning Research, vol 97. PMLR, pp 291–301, URL <https://proceedings.mlr.press/v97/anil19a.html>
- Björck A, Bowie C (1971) An iterative algorithm for computing the best estimate of an orthogonal matrix. SIAM Journal on Numerical Analysis 8(2):358–364. <https://doi.org/10.1137/0708036>
- Chernodub A, Nowicki D (2017) Norm-preserving orthogonal permutation linear unit activation functions (oplu). [1604.02313](https://arxiv.org/abs/1604.02313)
- Chizat L, Peyré G, Schmitzer B, et al (2018) Scaling algorithms for unbalanced optimal transport problems. Math Comp 87(314):2563–2609. <https://doi.org/10.1090/mcom/3303>
- Cuturi M (2013) Sinkhorn Distances: Lightspeed Computation of Optimal Transport. In: Burges CJC, Bottou L, Welling M, et al (eds) Advances in Neural Information Processing Systems, vol 26. Curran Associates, Inc., URL <https://proceedings.neurips.cc/paper/2013/file/af21d0c97db2e27e13572cbf59eb343d-Paper.pdf>
- Düll C, Gwiazda P, Marciniak-Czochra A, et al (2022) Spaces of measures and their applications to structured population models, Cambridge Monographs on Applied and Computational Mathematics, vol 36. Cambridge University Press, Cambridge
- Folland GB (1984) Real analysis. Pure and Applied Mathematics (New York), John Wiley & Sons, Inc., New York
- Geiger C, Kanzow C (2002) Theorie und Numerik Restringierter Optimierungsaufgaben. Masterclass, Springer Berlin, Heidelberg, <https://doi.org/10.1007/978-3-642-56004-0>
- Grauman K, Darrell T (2004) Fast contour matching using approximate earth mover’s distance. In: Proceedings of the 2004 IEEE Computer Society Conference on Computer Vision and Pattern Recognition, 2004. CVPR 2004., <https://doi.org/10.1109/CVPR.2004.1315035>

- Gulrajani I, Ahmed F, Arjovsky M, et al (2017) Improved training of Wasserstein GANs. In: Guyon I, Luxburg UV, Bengio S, et al (eds) Advances in Neural Information Processing Systems, vol 30. Curran Associates, Inc., URL [https://proceedings.neurips.cc/paper\\_files/paper/2017/file/892c3b1c6dcd52936e27cbd0ff683d6-Paper.pdf](https://proceedings.neurips.cc/paper_files/paper/2017/file/892c3b1c6dcd52936e27cbd0ff683d6-Paper.pdf)
- Gwiazda P, Marciniak-Czochra A, Thieme HR (2018) Measures under the flat norm as ordered normed vector space. Positivity 22(1):105–138. <https://doi.org/10.1007/s11117-017-0503-z>
- Kingma DP, Ba J (2015) Adam: A method for stochastic optimization. In: Bengio Y, LeCun Y (eds) 3rd International Conference on Learning Representations, ICLR 2015, San Diego, CA, USA, May 7-9, 2015, Conference Track Proceedings, URL <http://arxiv.org/abs/1412.6980>
- Lellmann J, Lorenz DA, Schönlieb C, et al (2014) Imaging with Kantorovich-Rubinstein discrepancy. SIAM J Imaging Sci 7(4):2833–2859. <https://doi.org/10.1137/140975528>
- Ling H, Okada K (2007) An efficient earth mover’s distance algorithm for robust histogram comparison. IEEE Transactions on Pattern Analysis and Machine Intelligence 29(5):840–853. <https://doi.org/10.1109/TPAMI.2007.1058>
- Peyré G, Cuturi M (2019) Computational optimal transport: With applications to data science. Foundations and Trends in Machine Learning 11(5-6):355–607. <https://doi.org/10.1561/22000000073>, URL <http://dx.doi.org/10.1561/22000000073>
- Peyré G, Fadili J, Rabin J (2012) Wasserstein active contours. In: 2012 19th IEEE International Conference on Image Processing, pp 2541–2544, <https://doi.org/10.1109/ICIP.2012.6467416>
- Piccoli B, Rossi F (2014) Generalized Wasserstein distance and its application to transport equations with source. Arch Ration Mech Anal 211(1):335–358. <https://doi.org/10.1007/s00205-013-0669-x>, URL <https://doi.org/10.1007/s00205-013-0669-x>
- Schiebinger G, Shu J, Tabaka M, et al (2019) Optimal-transport analysis of single-cell gene expression identifies developmental trajectories in reprogramming. Cell 176(4):928–943.e22. <https://doi.org/https://doi.org/10.1016/j.cell.2019.01.006>
- Tsuzuku Y, Sato I, Sugiyama M (2018) Lipschitz-margin training: Scalable certification of perturbation invariance for deep neural networks. In: Bengio S, Wallach H, Larochelle H, et al (eds) Advances in Neural Information Processing Systems, vol 31. Curran Associates, Inc., URL [https://proceedings.neurips.cc/paper\\_files/paper/2018/file/485843481a7edacbfce101ecb1e4d2a8-Paper.pdf](https://proceedings.neurips.cc/paper_files/paper/2018/file/485843481a7edacbfce101ecb1e4d2a8-Paper.pdf)
- Ulikowska A (2013) Structured population models in metric spaces. PhD thesis, University of Warsaw - Faculty of Mathematics, Informatics and Mechanics, URL

<https://depotuw.ceon.pl/handle/item/388>

Villani C (2003) Topics in optimal transportation, Graduate Studies in Mathematics, vol 58. American Mathematical Society, Providence, RI, <https://doi.org/10.1090/gsm/058>

Villani C (2009) Optimal transport- old and new, Fundamental Principles of Mathematical Sciences, vol 338. Springer-Verlag, Berlin, <https://doi.org/10.1007/978-3-540-71050-9>

Zappia L, Phipson B, Oshlack A (2017) Splatter: simulation of single-cell RNA sequencing data. Genome biology 18(1):1–15. <https://doi.org/10.1186/s13059-017-1305-0>

Zhang S, Afanassiev A, Greenstreet L, et al (2021) Optimal transport analysis reveals trajectories in steady-state systems. PLOS Computational Biology 17(12):1–29. <https://doi.org/10.1371/journal.pcbi.1009466>